communications materials

ARTICLE

https://doi.org/10.1038/s43246-021-00187-2 OPEN

Reducing crystallinity in solid polymer electrolytes for lithium-metal batteries via statistical copolymerization

Vincent St-Onge [1], Mengyang Cui [2], Sylviane Rochon[3], Jean-Christophe Daigle[3] & Jerome P. Claverie[1]✉

The discovery that polyethylene oxide promotes ionic conductivity led to the development of solid polymer electrolytes. However, their conductivity is severely reduced by crystallinity. Here, statistical copolymerization is used to design macromolecular architectures where crystallinity is disrupted by a minimal amount of non-ethylene oxide comonomer units. Using the Flory exclusion model, we demonstrate that polymers containing 18 mol% comonomer and 18 wt% LiTFSI are devoid of crystallinity. A 10 mol% comonomer content is sufficient to reach a conductivity of 0.3×10^{-4} S cm^{-1} at 25 °C. The Li^+ transference number is 0.6, indicating that the comonomer units not only limit the crystallinity but also weaken the strength of the Li^+ coordination to the polymer. The resulting solid polymer electrolyte is effective in an all-solid LFP|Li-metal battery operating at 25 °C, demonstrating that statistical copolymerization is an efficient tool for polymer electrolyte design.

[1] University of Sherbrooke, 2500 Boul. de l'Université, Sherbrooke, QC, Canada. [2] McMaster University, Hamilton, ON, Canada. [3] Center of Excellence in Transportation Electrification and Energy Storage, Varennes, QC, Canada. ✉email: jerome.claverie@usherbrooke.ca

Crystallinity is a fundamental characteristics of polymeric systems which defines mechanical, thermal, optical, electronic, and transport properties[1–5]. In the case of polyethylene oxide (PEO)—the archetypal solid polymer electrolyte (SPE) for Li^+ conduction—the presence of polymer crystallites which appear below the melting point ($T_m = 62$ °C for $M_n \sim$ 10–20 kg mol^{-1})[6–10] leads to a catastrophic collapse of ionic conductivity[11–13]. Electrolyte salts in SPE are excluded from polymer crystallites which are constituted of tightly packed polymer chains. Thus, each polymer crystallite *de facto* acts as an obstacle to salt diffusion and to ionic conductivity. Control over the polymer crystallinity is therefore of paramount importance to achieve ionic conductivity below 62 °C in PEO.

Many attempts at reducing PEO crystallinity can be found in the literature. The use of additives such as organic solvents (carbonates) to form gel polymer electrolytes (GPEs)[14–17] or longer organic molecules (small PEG, DOP) acting as plasticizers have been demonstrated to successfully disrupt the crystallinity. However, such materials, which are no more solvent-free, no longer provide the desired mechanical properties offered by all-solid-state PEO SPEs. A few all-solid-state polymer electrolytes (ASSPEs) can be found in the literature, being the results of composite polymer electrolytes (CPEs)[18], polymer blends (like PEO with PVDF)[19] or (semi-) interpenetrating networks[20]. They offer promising avenues where the PEO chains are kinetically trapped either in a crosslinked matrix of another polymer or in the surrounding of inorganic particles, thus delaying crystallization of the PEO chains. However, to our knowledge, this strategy did not lead to a battery functioning at room temperature. Thus, it is necessary to address PEO crystallinity at the molecular level to prohibit the formation of crystallites and to allow the fabrication of ASSPE functioning at room temperature.

A crystallite can be viewed as a nanometric lamella in which polymer chains are oriented orthogonally to the lamellae facets (Fig. 1)[6,21]. There is no space to accommodate any defect such as a comonomer unit or a chain-end inside the crystallite. Thus, defects are concentrated in the amorphous region. This representation of polymer crystals constitutes the central premise of the Flory exclusion model[22,23]. The lamellar thickness is limited by the distance between two defects placed along the polymer chain. Increasing the frequency of defects results in smaller crystallites, which in turn affects the T_m of the crystallized polymer, as stated by the Gibbs–Thomson equation[24,25].

In statistical copolymerization, the distribution of comonomer units follow a statistical law without any recurring arrangement. In such a copolymer, it only takes a few comonomer units to significantly disrupt the crystallinity because the thickness of an entire crystallite is limited by the length of the shortest PEO sequence between two monomers located on either facet of the crystallite, even though many longer sequences exist (Fig. 1)[26,27]. Therefore, statistical copolymerization is a potent tool to prevent the crystallization of a polymer. This technique is remarkably suited to prepare PEO-based SPE, as PEO units must be kept in the largest possible amount to efficiently complex and dissolve lithium cations responsible for ionic conductivity, while crystallinity must be kept as low as possible. To our knowledge, no study exists on the tuning of the PEO crystallinity through statistical copolymerization. Therefore, a fundamental question that is addressed here lies in the determination of the smallest amount of comonomer needed to break crystallinity. From this knowledge, a PEO rich material, which favors ionic conductivity, can be prepared with a minimal amount of comonomer units (defects) to prevent crystallization[28].

To answer this work hypothesis, three families of statistical copolymers (Fig. 1) were prepared, and it was discovered that *ca* 26 mol% of comonomer was sufficient to entirely obliterate polymer crystallinity leading to a PEO-rich material that is thermodynamically unable to crystallize. The Li^+ conductivity of these novel materials was assessed, and unlike pure PEO, their

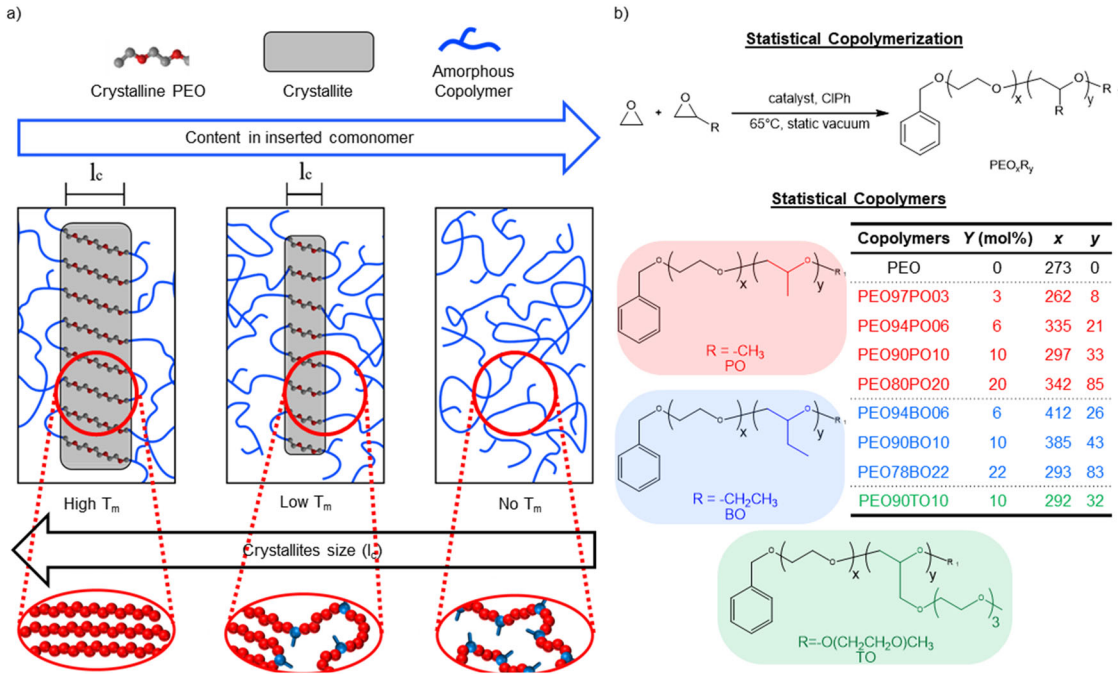

Copolymers	Y (mol%)	x	y
PEO	0	273	0
PEO97PO03	3	262	8
PEO94PO06	6	335	21
PEO90PO10	10	297	33
PEO80PO20	20	342	85
PEO94BO06	6	412	26
PEO90BO10	10	385	43
PEO78BO22	22	293	83
PEO90TO10	10	292	32

Fig. 1 Schematic representation of copolymer crystallinity. a Breaking of crystallinity with increased comonomer content, resulting in reduced crystallites size and lower melting temperature, and eventually leading to loss of crystallites, hence no crystallinity and no observable melting temperature. Sketches (in red ovals) represent the molecular arrangements with comonomer content. Ethylene oxide units are represented by red spheres and substituted epoxides by blue spheres with the substituent depicted as a blue bar. **b** General synthetic pathway for the design of statistical copolymers of ethylene oxide and substituted epoxides, including molecular structures of the three families of copolymers synthesized, along with their compositions.

conductivity remains elevated at 25 °C. Remarkably, the presence of the statistical defects not only prevent crystallization, but also decreases the strength of the PEO—Li^+ coordination, resulting in Li^+ transference numbers that can be as high as 0.58, as opposed to 0.21 for PEO homopolymer. Using such materials, an all-solid-state battery was fabricated, using metallic Li as anode, and lithium iron phosphate (LFP) as cathode. At ambient temperature (25 °C), the battery exhibits a capacity as high as 120 mAh g^{-1}, and does not show any sign of degradation, even after an excursion at C/3 rate. Thus, by their high conductivity and high transference numbers at ambient temperature, these PEO statistical copolymers are highly promising materials for the fabrication of all solid-state Li batteries, thus solving the dilemma between temperature and conductivity.

Results and discussion

Structural and thermal properties. The statistical copolymers of ethylene oxide with substituted oxiranes were prepared according to the pathway described in Fig. 1 (experimental details in Supplementary Table 1). Analysis of the copolymer composition by ^{1}H nuclear magnetic resonance (NMR) demonstrates that each copolymer contains around 300 EO units and a few comonomer units which increases with comonomer feed (see Fig. 1 and Supplementary Fig. 1 for copolymer composition control, and Supplementary Figs. 2–13 for NMR analysis). Microstructural analysis of the comonomer distribution units was assessed using quantitative ^{13}C NMR (see Supplementary Figs. 3–9, Supplementary Tables 2–5, and Supplementary Notes 2–4)[29–32]. From these data, it is possible to extract the reactivity ratios of EO ($r_1 = 0.11$) and propylene oxide (PO, $r_2 = 0.01$) for the copolymerization of EO and PO, and the reactivity ratios of EO ($r_1 = 0.01$) and butylene oxide (BO, $r_2 = 0.0001$) for the copolymerization of EO and BO (for Finemann–Ross fitting models, see Supplementary Fig. 1 and Supplementary Note 1). These reactivity ratios indicate that PO or BO comonomer units are isolated between linear sequences of EO units. Such microstructure is ideal to favor high conductivity since only one comonomer unit is necessary to stop the crystallization of an EO sequence. Two or more PO comonomers in a row would reduce the ionic conductivity because a comonomer unit is not able to solvate the Li^+ cation as well as EO units, as suggested by the much lower ionic conductivity of poly(propylene oxide) (PPO) under similar conditions as opposed to that of PEO with lithium bis-(trifluoromethane sulfonyl)imide (LiTFSI)[33,34].

As shown in Fig. 2b, the statistical copolymer containing 26 mol% PO or BO units is devoid of crystallinity. In such copolymers, the average EO sequence is 3 units long indicating that 3 EO units in a row are too short to induce crystallization. Since CH_3 and C_2H_5 side chains do not contribute to ionic conductivity, it is advantageous to replace these hydrocarbon side chains by short EO sequences (length ≤ 3 units) that are unable to crystallize. Thus, statistical copolymers with TO, a monomer with a pendant group of 3 EO units, were also investigated.

The thermal properties of the copolymers were determined by modulated differential scanning calorimetry (mDSC, Fig. 2a). Two thermal phase transitions can be observed, the glass transition, T_g, at low temperature, and the melting point, T_m, at higher temperature. Below T_g, chain reptation is not allowed and ionic conductivity is practically null. Thus, T_g (typically comprised between −80 and −50 °C) defines the lowest usage temperature for a SPE. If the copolymer exhibits some crystallinity, as shown by an endothermic melting peak in mDSC, its crystallinity content (volume fraction of crystallites) can be conveniently assessed by integration of the melting peak (see Supplementary Table 1 and Supplementary Fig. 14–29), using $\Delta H_m \sim 213\ J\ g^{-1}$ [10]). In pure PEO, crystallinity is around 60–80% depending on molecular weight and processing conditions. In such homopolymers, the amount of amorphous phase is not sufficient to ensure ionic conductivity, and the polymer can only be used as SPE in the liquid state ($T > T_m$). Statistical copolymers exhibit a lower T_g, a lower T_m and a lower crystallinity content as opposed to pure PEO, all of which are expected to increase the temperature range at which they can be used as SPE. Longer side chains (PO < BO < TO) have a more pronounced effect on the decrease of T_g, which can be ascribed to a self-plasticization effect.

The melting transition of the copolymers is characterized by a broad peak which is shifted to lower temperature compared to PEO. Such phenomenon is captured by the Gibbs–Thomson equation (Eq. (1), with γ being the interfacial tension between crystallites and amorphous phase, and V being the molar volume of the crystallizable unit) which states that the depression of the melting point ($\Delta T_m = T_m - T_m^0$, T_m^0 corresponding to the melting point of pure PEO in bulk) is inversely proportional to crystal size (l), so that smaller crystals melt at lower temperature[6]. The introduction of comonomers limits the crystallite size, resulting in a notable decrease in melting point (as was depicted in Fig. 1). While PEO melts at 62 °C, copolymers containing 10 mol% of PO and BO melt at 47 and 55 °C, respectively. This decrease in melting point is accompanied by a drastic decrease in

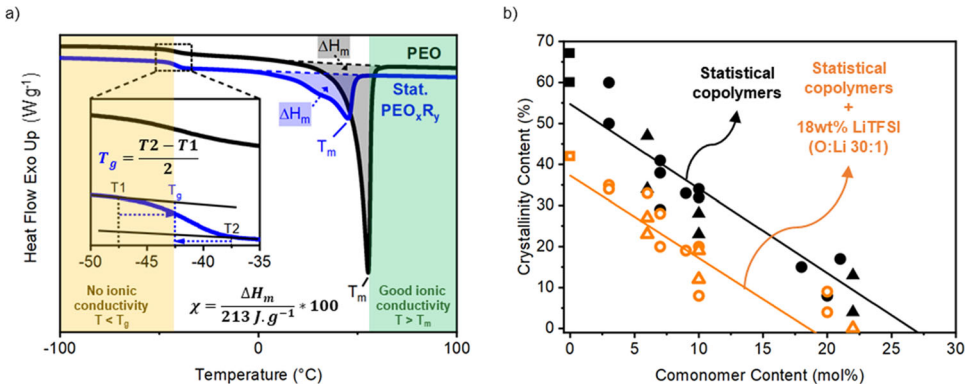

Fig. 2 Thermal characterization of materials. a Thermogram for polyethylene oxide (PEO) (black curve) and for a typical statistical copolymer (blue curve). **b** Crystallinity content versus comonomer content, for statistical copolymers with (orange) and without (black) 18 wt% lithium bis-(trifluoromethanesulfonyl)imide (LiTFSI), where squares are for PEO, circles are for copolymers of ethylene oxide with propylene oxide (PEOPO) and triangles are for copolymers of ethylene oxide with 1,2-butylene oxide (PEOBO).

crystallinity content (60%, 33 and 28% for PEO, PEOPO, and PEOBO copolymers, respectively).

$$\triangle T_m = T_m - T_m^0 = \left(1 - \frac{2 \cdot \gamma \cdot V}{l \cdot \triangle h}\right) \quad (1)$$

The crystallinity content versus comonomer molar content is illustrated in Fig. 2b. All copolymers follow the same linear regression no matter the nature of the side chains. Such behavior is explained by the fact that the crystal size is a colligative property in the Flory exclusion model, meaning that it is only affected by the frequency of defects (comonomers) and not by their nature. The crystallinity content of a polymer theoretically depends on its thermal history. Thus, we also measured these values by powder X-ray diffraction (pXRD) at room temperature (see Supplementary Figs. 30–34 for diffractograms), by contrast to mDSC (second heating ramp) which requires to heat the sample. In our case, both types of analyses yield similar values. Extrapolating crystallinity values versus comonomer content (Fig. 2b), it can be inferred that copolymers containing 26 mol% of any comonomer units is unable to crystallize.

The crystallinity of PEO SPEs is affected by the presence of salts, which can be explained by the well-known effect of melting point depression for an impure solid. Indeed, the formation of a PEO crystal would require to concentrate the salt within the amorphous phase, which is energetically unfavorable[35]. Such effect is for example observed in SPEs with very high salt concentrations (>50 wt%), namely polymer-in-salt SPEs[36]. In such regime, all oxygen atoms in the polymer chain are coordinated to Li^+, preventing the packing of PEO chains in a crystallite. In this work, we deliberately chose lower salt concentrations (18 wt% LiTFSI, corresponding to 30:1 O:Li) not only to favor an economically viable SPE, as LiTFSI is expensive, but also because this low concentration in salt has been reported to give the highest ionic conductivities for salt-in-polymer PEO SPE[37].

As expected, the crystallinity content of the copolymers containing 18 wt% LiTFSI (Fig. 2b, orange data) is lower than the one of the pure copolymers (Fig. 2b, black data). With this salt concentration, crystallinity is thermodynamically absent in copolymers containing at least 18 mol% of comonomer (versus 26 mol% in the absence of LiTFSI). The presence of LiTFSI also results in an increase in T_g (from −70 °C to −50 °C for 10 mol% of BO units). This phenomenon can be explained by the fact that lithium coordination restricts chain mobility in the amorphous phase[38]. This increase in T_g is nonetheless sufficiently low to allow the use of this statistical copolymer-based SPE under typical environmental conditions. To conclude this section, we have demonstrated that statistical copolymers containing 18 mol% of comonomers with 18 wt% of LiTFSI are entirely devoid of crystallinity.

Ion transport behaviors. Ionic conductivity measurements of the SPEs with LiTFSI were performed by means of electrochemical impedance spectroscopy (EIS, reported in Supplementary Note 6 and Supplementary Figs. 38–48) to select the best candidate for coin cell cycling (Fig. 3). The equivalent electric circuit used to fit the EIS data are shown in Fig. 3a, along with the quick calculation for the determination of the SPE resistance (R). Remarkably, the ionic conductivities of the copolymers are two to three orders of magnitude higher than that of pure PEO at 25 °C. There is only a small difference for the conductivity of the copolymers containing PO (Fig. 3b) and BO units (Fig. 3c), demonstrating that the ionic conductivity is mainly due to the EO units with little influence from the nature of the comonomer side group. Contrasting with the nature of the comonomer side chain, the comonomer content strongly impacts ionic conductivity (Fig. 3e), which is in good agreement with the colligative nature of copolymer crystallinity, as stated in the Flory exclusion model. A low amount of comonomer results in a decrease of crystallite size and decrease in crystallinity content. Consequently, the ionic conductivity grows from 5×10^{-8} to 0.3×10^{-4} S cm^{-1} by only adding 10 mol% of comonomer (Fig. 3d, e). Introducing larger amounts of comonomer in the SPE results in a conductivity drop, because the comonomers are not as efficient as EO units to dissolve and complex the Li^+ salt. Thus, 10 mol% of comonomer units in the copolymer offers is the best compromise between reducing the crystallinity and increasing the EO content necessary for ionic conductivity. These copolymers have crystallinity contents of 19%, 12, and 4%, and T_gs of −44 °C, −50 °C, and −72 °C for PO, BO, and TO units, respectively. Therefore, all further analyses were performed on copolymers containing 10 mol% in comonomer content. To rule out any influence coming from residual solvents on the measured ionic conductivity[39], thermogravimetric analysis was performed on the SPEs (see Supplementary Note 5 and thermogravimetric analysis (TGA) curves in Supplementary Figs. 35–37). All samples were devoid of residual solvent, thus proving that the change in ionic conductivity really comes from comonomer insertion and crystallinity tuning. At room temperature, the best ionic conductivity is obtained with the copolymer containing TO units (PEO90TO10-18Li). Indeed, this copolymer has 10 mol% of comonomer, but it is constituted of 97.5 mol% EO units (PEO90TO10, since 3 units out of 4 of the TO comonomer are also EO), thus allowing the highest ionic conductivity. As seen in Fig. 3f, there is barely any difference in ionic conductivity for copolymers containing either 18 or 30 wt% LiTFSI, which is advantageous from an economical standpoint.

Remarkably, ionic conductivity with the statistical copolymers exhibit a single activation energy behavior for temperature range between 25 °C and 75 °C, while in contrast, PEO has a high activation energy (Ea = 116 kJ mol^{-1}) below its T_m (62 °C) and a low activation energy (Ea = 40 kJ mol^{-1}) above T_m, in good agreement with literature values reported for PEO-LiTFSI[40–42]. For copolymers with 10 mol% of either PO, BO, and TO, the activation energy is respectively 58, 72, and 44 kJ mol^{-1} (Fig. 3a–c, see Supplementary Table 6 for activation energies of the other copolymers). These low values of activation energy confirm our work hypothesis that tuning the crystallinity with a low amount of comonomer units is an efficient tool to control ionic conductivity.

The transference number from potentiostatic polarization measurements (Fig. 4a) further shine light on the ionic conductivity of the statistical copolymers. The low Li^+ transference number in PEO-based SPEs ($t_{Li+} = 0.21$, Fig. 4a) is attributed the strong coordination of the cations by the oxygen atoms from the polyether (Fig. 4c). In an operating Li-battery, a low cationic transference number is associated with undesirable effects, such as polarization of the cell, resulting in an increase of its resistivity, and even dendrite formation, leading to catastrophic battery failure[43,44], Remarkably, the Li^+ transference numbers of copolymers containing PO and BO units are substantially greater. This phenomenon can be ascribed to the presence of non-EO side chains, which are unable to coordinate the lithium cations. Between four to seven oxygen atoms are involved in the Li^+ coordination in EO-based materials (Fig. 4c)[45]. When such oxygen atoms are within a polymer chain, the energetically favorable coordination is partially counterbalanced by a conformational entropic penalty. Obviously, the presence of alkyl substituents that cannot approach the ionic species will reinforce this entropic cost, making the coordination weaker (Fig. 4d). For copolymers containing TO units, the situation is reversed. Since the TO units have pre-organised EO substituents, efficient coordination of Li^+ cations by the polymer does not require a large conformational entropic cost. In short, the

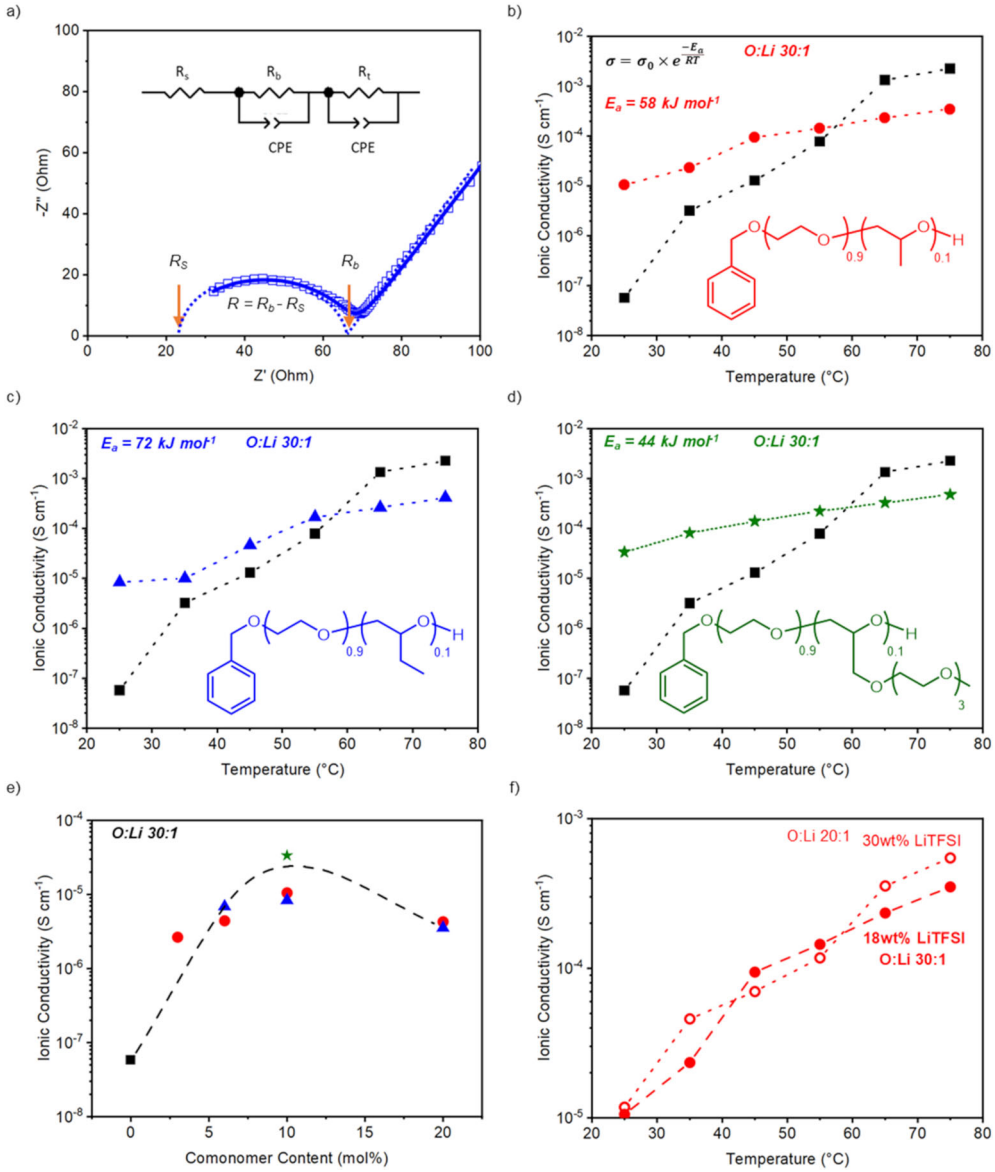

Fig. 3 Ionic conductivities of solid polymer electrolytes. a Graphical view of complex impedance graph obtained from electrochemical impedance spectroscopy (EIS) measurement, with experimental data (hollow square), fitted data (solid blue line), and extension of fitted curve (dashed blue line), calculated from the equivalent electronic circuit above the data. **b** Ionic conductivities vs temperature for sample PEO90PO10-18Li (in red) **c** sample PEO90BO10-18Li (in blue) **d** and sample PEO90TO10-18Li (in green), compared to sample PEO-18Li (in black). **e** Room temperature ionic conductivity vs comonomer content (polyethylene oxide (PEO) in black, copolymers of ethylene oxide with propylene oxide (PEOPO) in red, copolymers of ethylene oxide with 1,2-butylene oxide (PEOBO) in blue and copolymers of ethylene oxide with methyl ether triethylene glycol glycidyl ether (PEOTO) in green). **f** A comparison between the ionic conductivities of 18 wt% (full symbols) and 30 wt% (hollow symbols) lithium bis-(trifluoromethanesulfonyl)imide (LiTFSI) in sample PEO90PO10 vs temperature.

copolymers containing 3 EO pendant branches behaves like a cryptand (Fig. 4e), leading to a Li^+ coordination which is reinforced by a chelating effect[46]. Importantly, this behavior is confirmed by measuring self-diffusion coefficients obtained by ^{7}Li and ^{19}F pulse-field gradient solid-state nuclear magnetic resonance spectroscopy (PFG SSNMR).

The self-diffusion coefficients, presented in Fig. 4b, extracted from ^{7}Li and ^{19}F PFG SSNMR experiments performed at 45 °C, showed a substantial increase for the copolymers compared to that in PEO (see Supplementary Fig. 49–53 for the fitting of the attenuation curves). Self-diffusion coefficients and conductivities are related through the Nernst-Einstein equation, hence higher diffusion coefficients usually lead to higher ionic conductivities. This is in good agreement with the measured ionic conductivities at room temperature, with all 3 copolymers having higher conductivity values and PEOTO being the highest. The degree of salt dissociation can be estimated from self-diffusion coefficients obtained by NMR and ionic conductivity obtained by impedance spectroscopy, to give the ideality parameter β (Eq. (2)), which are reported in Supplementary Fig. 49[47].

$$\beta = \frac{\sigma RT}{F^2 c(D_+^{NMR} + D_-^{NMR})} = \frac{\sigma RT}{F^2 c(D_{Li} + D_F)} \quad (2)$$

Values close to 0 for this parameter indicates that the salt has a low dissociation degree, whereas values close to unity are observed for an ideal electrolyte in which the anion and the cation are fully dissociated. Remarkably, this value reaches 1.3 for copolymers containing 10 mol% of PO while it is 0.5 for PEO

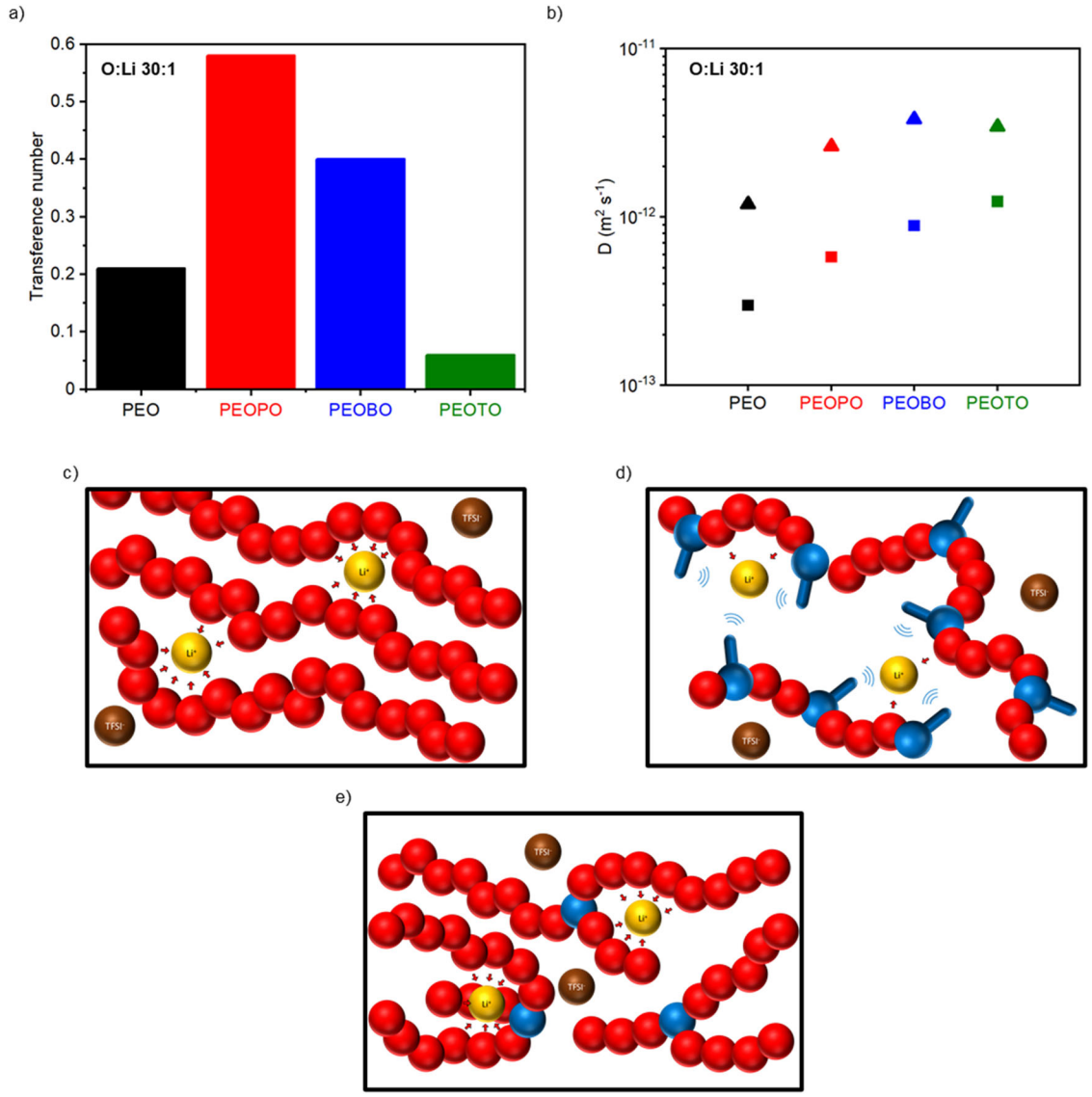

Fig. 4 Characterization of the ionic transport. a Cationic transference numbers of statistical copolymers (10 mol% comonomer) obtained by the Bruce–Vincent method at 25 °C. **b** Self-diffusion coefficients obtained by PFG-SSNMR (square for lithium and triangle for fluorine). Schematized representation of the coordination of Li^+ (yellow sphere) **c** in polyethylene oxide (PEO), **d** in copolymers of ethylene oxide with propylene oxide (PEOPO, comonomer unit in blue) and **e** in copolymers of ethylene oxide with methyl ether triethylene glycol glycidyl ether (PEOTO).

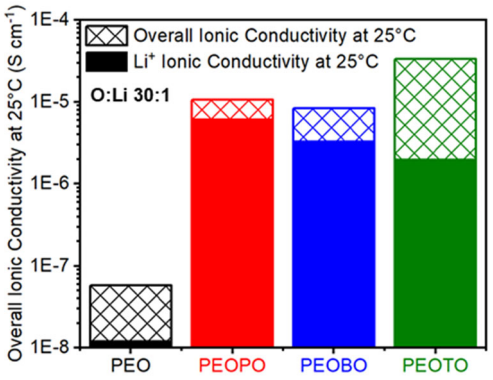

Fig. 5 Overall and Li^+ ionic conductivities at 25 °C. Overall ionic conductivity (solid bars, measured by NMR) and Li^+ ionic conductivity (patterned bars, measured electrochemically) at 25 °C for polyethylene oxide (PEO, black) and for copolymers containing 10 mol% of propylene oxide (PO, red), 1,2-butylene oxide (BO, blue), and methyl ether triethylene glycol glycidyl ether (TO, green).

(Supplementary Fig. 54). This result is in good agreement with the high ionic conductivities and cationic transference numbers that are measured for such copolymers. In SPEs, it is necessary to find a compromise between dissolution of the salt, which is favored by a strong coordination of the cations, and mobility of the Li^+ within the polymer, which is on the contrary favored by the absence of coordination.

With the highest value of Li^+ ionic conductivity (as shown in Fig. 5), high values of overall ionic conductivity, lithium transference number and ideality parameter, the statistical copolymer of EO with PO (10 mol%) offers the optimal balance between these conflicting parameters. Hence, this copolymer was chosen for battery testing.

Battery testing. To test the efficiency of our SPE material, we decided to use lithium iron phosphate (LFP) as the active cathode material[48,49] and metallic lithium as the anode material. Such configuration is more challenging than with the graphitic anode because dendrites can grow on the lithium anode and the output

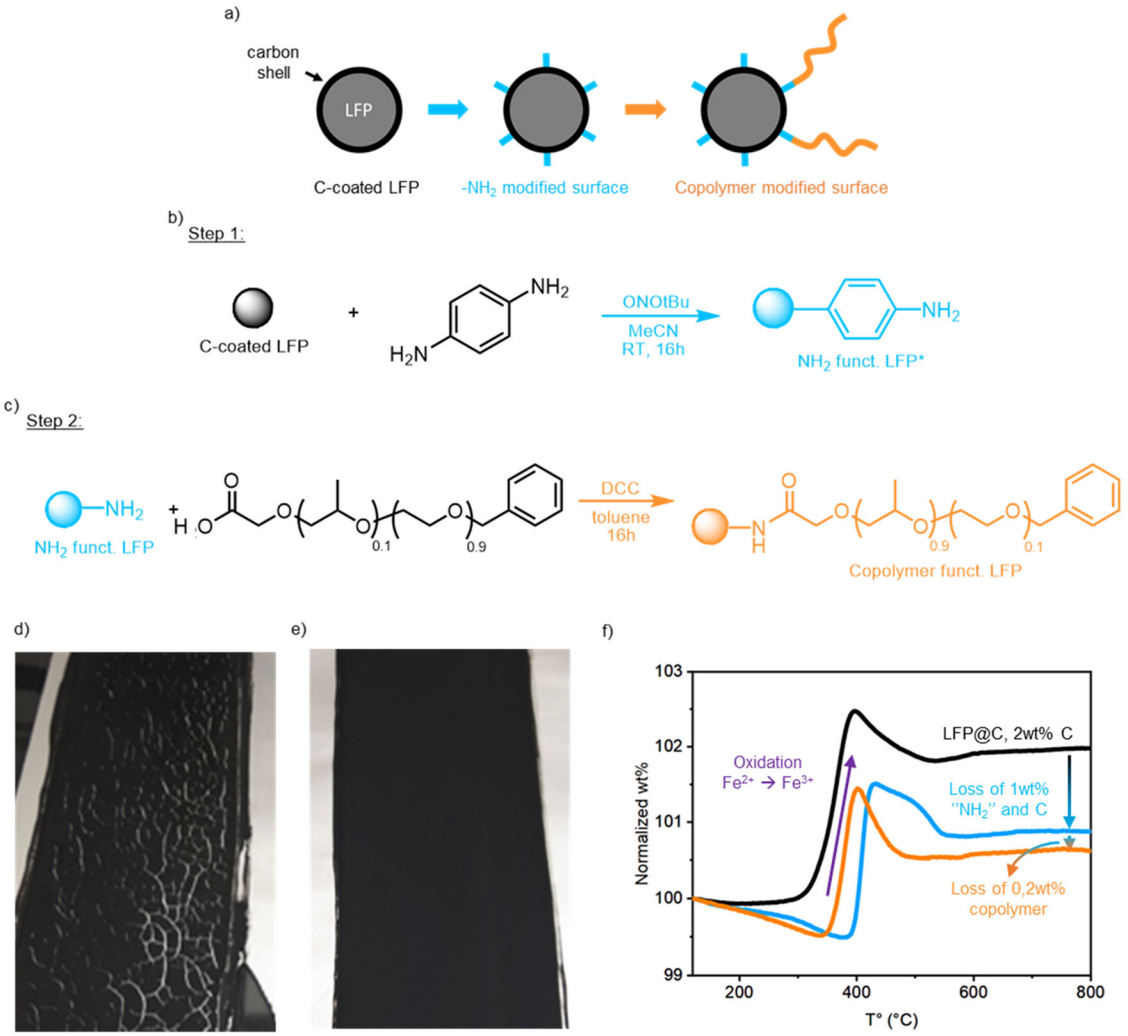

Fig. 6 Carbon-coated lithium iron phosphate (C-coated LFP) particles surface functionalization. a Schematized general procedure. **b** Step 1: NH_2 functionalization (step 1, following literature procedure[51]). **c** Step 2: copolymer grafting onto amine functionalized C-coated LFP particles (step 2). **d** Picture of C-coated LFP coating on aluminum current collector. **e** Picture of functionalized C-coated LFP on aluminum current collectors. **f** Thermogravimetric analysis of C-coated LFP particles (black), after -NH_2 modification (light blue) and after copolymer grafting (orange).

voltage is higher by *ca.* 200–300 mV, therefore, requiring larger electrochemical stability window. However, the use of metallic lithium offers several advantages, namely a very large theoretical specific capacity, and a higher energy density resulting from the higher output voltage[50]. To our knowledge, there is no report of an all-solid lithium-metal polymer battery with LFP cathode functioning at room temperature.

To address this challenge, the LFP-based cathode was first prepared from a slurry containing carbon-coated LFP particles, LiTFSI, carbon black, and a binder (polyvinylidene fluoride, PVdF, carboxymethylcellulose, CMC, PEO, or our copolymer). In all cases, such formulations led to poor results due to an absence of adhesion, either with the SPE (PVdF, CMC) or with the current collector (PEO, copolymer, Fig. 6d). Such undesirable results can be explained by the lack of compatibility between carbon-coated LFP particles and the SPE, which leads to macrophase separation. To solve this issue, the surface of the LFP@C particles was grafted with the copolymer to ensure compatibility (Fig. 6a). This grafting was performed via a two-step procedure whereby surface NH_2 groups were first introduced using diazo chemistry (Fig. 6b)[51], followed by an amidification with copolymer chains which were end-capped by CO_2H groups (Fig. 6c). Proof of grafting is obtained by thermal gravimetric analysis which shows that 0.2 wt% of copolymer is grafted at the surface of the particle (Fig. 6f). The presence of grafted copolymer drastically affects the surface properties of the particles. As shown in Fig. 6e, the LFP slurry with grafted copolymer yields a smooth defect-free film on the current collector, which was then used as cathode in coin cell batteries.

Before testing in battery, the electrochemical stability of our statistical copolymer-based SPE was assessed by linear sweep voltammetry (Fig. 7a) and cyclic voltammetry (Supplementary Fig. 55) between two lithium blocking electrodes. No degradation is observed up to 8 V (vs Li^+/Li) by LSV, nor upon cycling by CV between −0.5 and 4 V, ensuring that our SPE is stable for the cycling process. At room temperature, the LFP|SPE|Li batteries (Fig. 7b) charged up to 3.75 V exhibited a discharge plateau at the value of 3.4 V corresponding to the expected potential difference for LFP vs Li cell (Supplementary Fig. 56).

After the SEI formation, the specific capacity of the LFP|SPE|Li batteries remain high (up to 120 mAh g^{-1}) with only a 20% capacity drop at the faster C/3 rate (Fig. 7c). The specific capacity is recovered with slower charging rates, indicating that the drop of specific capacity is only due to a slightly diminished kinetic performance, but not to degradation. Furthermore, after 30 cycles, the coulombic efficiency remains at 100% (excepted at SEI

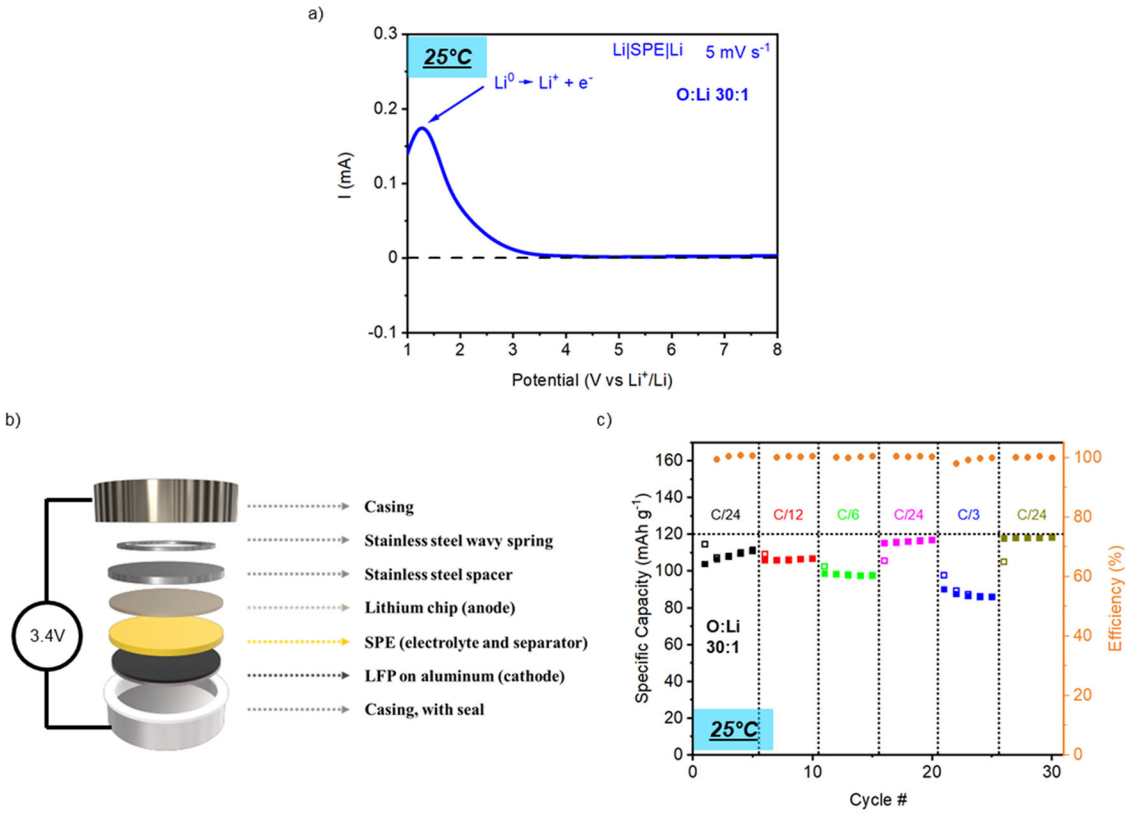

Fig. 7 Electrochemical testing of the PEO90PO10 solid polymer electrolyte (SPE) at 25 °C. a Linear sweep voltammetry (LSV) curve obtained for the PEO90PO10 SPE with O:Li ratio of 30:1, between 2 lithium electrodes, from 1 to 8 V at a scan rate of 5 mV s^{-1}. **b** Schematic description of the battery. **c** Specific capacities (black axis and square data) and coulombic efficiencies (orange axis and orange round data) of the batteries are presented for each cycle, for both charge (hollow symbols) and discharge (full symbols), with colors corresponding to various C-rates (C/24 in black, C/12 in red, C/6 in light green, C/24 (2nd time) in magenta, C/3 in blue, and C/24 (3rd time) in gold).

forming steps, Fig. 7c), once again indicating the high stability of the battery. At regular intervals, the LFP|SPE|Li batteries were further characterized by EIS, which allows to characterize the charge transfer resistance within the SPE. The first cycle leads to a 1.3% increase of the charge transfer resistance, corresponding to the SEI formation. Subsequently, the values of charge resistance remain constant, indicating that the ionic conductivity within the SPE is not affected by the cycling (Supplementary Fig. 57). Further evidence of the stability has been obtained by means of galvanostatic experiments[52], demonstrating the efficiency of our optimized SPE compared to PEO SPE (see Supplementary Fig. 58). Thus, these all-solid LFP|SPE|Li batteries are efficient at ambient temperature, delivering a stable 3.4 V operating voltage, and with no decrease of performance after 30 charge-discharge cycles.

Conclusion. Crystallinity is a major barrier to ionic conductivity in solid polymer electrolytes. Using the Flory exclusion model, statistical copolymerization is found to be a remarkably efficient tool to lower crystallinity. Thanks to this tool, copolymers of EO that are ionically conductive at room temperature were unraveled. Due to the colligative nature of the crystallinity, ionic conductivity was found to be mostly dependent on copolymer composition, but it was little affected by the nature of the comonomer. Thus, for the three family of copolymers assessed, the highest ionic conductivity (up to 0.3×10^{-4} S cm^{-1} at room temperature with 18 wt% LiTFSI) was reached when the copolymer contained 10 mol% of comonomer. Although conductivity was little affected by the nature of the comonomer, Li^+ transference number was in turn critically dependent upon it. Thus, values of 0.1 and 0.6 were reached for the EO-TO and EO-PO statistical copolymers respectively, indicative that statistical copolymerization offers a unique potential to tune this important parameter. The EO-PO copolymer was used as SPE a first example of an all-solid Li-metal battery operating at 25 °C. With a specific capacity of 120 mAh g^{-1}, the battery operates with high coulombic efficiency and no visible loss of capacity, even after excursions at C/3 rate. Thus, statistical copolymerization is a compelling technique to design SPEs.

Methods

Materials. Ethylene oxide was bought from Praxair Canada and condensed in a specially designed thick-glass container on CaH_2, then cryo-distilled prior every use. Racemic propylene oxide and 1,2-butylene oxide were bought from Fisher Scientific Canada. They were dried and distilled over CaH_2, then stored in a nitrogen-filled glovebox prior to use. Triethyl aluminum (93%) was bought from Sigma-Millipore and used as received, in a nitrogen-filled glovebox. Benzyl alcohol, toluene, anhydrous tetrahydrofuran (THF) was distilled over CaH_2 and stored in a nitrogen-filled glovebox. Silica (Davisil grade 636, 60 Å pores, 35–60 mesh particles size) was bought from Sigma-Millipore and dehydrated in a tubular oven at 200 °C, then stored in a nitrogen-filled glovebox prior to use. Chlorobenzene was bought from Sigma-Millipore and dried over K_2CO_3, distilled under reduced pressure, then stored in a nitrogen-filled glovebox over 4 Å molecular sieves prior to use. Carbon-coated LFP and LiTFSI were kindly provided by the Center of Excellence in Transportation Electrification and Energy Storage – Hydro-Québec (Varennes, QC, Canada) and used as received.

Catalyst synthesis procedure. The heterogeneous catalyst for ring-opening statistical copolymerization was prepared according to the work of Hamaide et al.[53]. Under inert atmosphere, triethyl aluminum (0.6 mL) was added dropwise to a dispersion of dehydrated silica (0.5 g) in dried toluene (10 mL). The mixture was left to stir at room temperature for 30 min, then benzyl alcohol (6 mL) was added dropwise. The reaction was then brought to 45 °C and stirred for 2 h. The mixture was then left to decant at room temperature and the excess liquid was removed.

The discarded solution was quenched with alcohol prior disposal. The catalyst slurry was suspended in another portion of dried toluene (10 mL), stirred, then left to decant and excess liquid was removed and quenched carefully. This procedure was repeated twice, then the catalyst was dried at 40 °C under vacuum (14 mbar) for 15 min, then kept stored under inert atmosphere.

Co-catalyst synthesis procedure. In a glovebox, triethyl aluminum (6 mL) was added dropwise to a solution of BHT (2 g) in toluene (20 mL) and left to stir for 4 h to give a solution of the co-catalyst at a concentration of around 0.1 M in toluene. This solution was used as is.

Typical procedure for copolymerization. The manipulation of EO can be hazardous and should only be performed by highly skilled experimenter. Due to the toxicity of the monomers, all residual solvents and unreacted monomers must be quenched with hydrochloric acid before discarding them to waste. In a glovebox, a half-jacketed 3-neck round bottom flask made of thick glass for pressure handling was equipped with a magnetic stirring bar, 2 septa, and a vacuum connector. Then, catalyst (0.1–0.4 g), co-catalyst (1–4 mL required TO monomer), and chlorobenzene (80–150 mL) were added. The mixture was frozen in a liquid nitrogen bath, then the comonomer (1–40 mL) was added and left to freeze. The system was placed under static vacuum (150 µm Hg), then the mixture was brought back to room temperature. While there was still some frozen solvent in the mixture, ethylene oxide (0.5–3.5 mL) was added. The mixture was then brought to 65 °C (the pressure buildup in the flask was monitored with a pressure sensor to avoid over-pressure and breaking the glassware). The copolymerization was left to react for 24 h, then the connectors were removed while the flask was under a flux of nitrogen. The unreacted monomers were left to evaporate, then the copolymer was precipitated with 600 mL of hexanes and filtered. The precipitated polymer was dried under vacuum at room temperature for 24 h to give a white-yellowish powder.

General procedure for polymer electrolytes preparation. In a nitrogen-filled glovebox, 820 mg of polymer was dissolved in 5–10 mL of anhydrous THF. Then, 180 mg of LiTFSI was added to the solution and dissolved at 65 °C. The solvent was then evaporated under reduced pressure and dried under vacuum for 24 h. The electrolyte was kept in the nitrogen glovebox.

General procedure for TGA. In a TGA crucible, ~15 mg of materials was weighted, then the crucible was placed on the TGA balance. TGA was performed on a Perkin Elmer TGA 4000. The atmosphere was then purged with argon (for residual solvent characterization; left under air for LFP grafting characterization), then the sample weight was tarred, and the sample was heated at 10 °C min^{-1} from room temperature up to 500 °C. TGA curves were reported in wt% compared to the initial weight.

General procedure for ionic conductivity measurements. Conductivity measurements were performed in the glovebox to avoid the presence of water and oxygen. The SPE was first heated at 90 °C for 1 h, then brought back at 25 °C prior to any measurement. The assembled cell containing the polymer electrolyte was placed in a measurement cell constituted of a thermostated press[54]. A high pressure (P = 1 ton) was first applied to ensure removal of any gas traces, then the pressure was released to leave only a small pressure (P = 0.1 ton) on the cell (to ensure electrodes/electrolyte contact). Measurements were carried on with an AC amplitude of 10 mV at a constant potential of 0 V versus OCP with a Zahner Elektrik Zennium system, between 25 and 80 °C, 5 °C stepwise.

General procedure for lithium transference number measurements. In a symmetric coin cell (CR2032), the polymer electrolytes were sandwiched in between two lithium chips (15.4 mm d., 0.45 mm t.). The assembled coin cell was then heated at 70 °C for 1 h to ensure good electrodes/electrolytes contact. Determination of initial and steady-state current was done using chronoamperometry with a DC bias of 0.01 V for 24 h. Determination of initial and steady-state electrolytes resistance was done using electrochemical impedance spectroscopy, with a 0.01 V DC bias and an AC amplitude of 10 mV.

DSC measurements. DSC pans were assembled in a nitrogen-filled glovebox. Measurements were carried on a TA Instruments DSC2500 with an auto-sampler, from 120 °C to 120 °C, with a temperature ramp of 10 °C min^{-1} both during upon heating and cooling. The reported measurements correspond to the second heating.

XRD Measurements. Measurements were carried on a Panalytical X'Pert Pro diffractometer and a copper source. The diffractograms were acquired between 10 and 30 degrees 2θ for analysis of the region of interest.

^{1}H NMR experiments. ^{1}H NMR spectra were acquired on a Bruker AVANCE III 300 MHz spectrometer at a concentration of 10 mg mL^{-1} in $CDCl_3$.

Quantitative ^{13}C NMR experiments. ^{13}C NMR spectra were recorded on a Varian 400 MHz spectrometer at a concentration of 200 mg mL^{-1} in $CDCl_3$ to determine the microstructure of the polymer chains (statistical analysis of monomers distribution). The acquisition was made using an inverse gated proton decoupling pulse sequence and a relaxation delay of 10 s. A total of 4096 scans were acquired for each sample.

Self-diffusion by PFG SSNMR. Diffusion measurements with the pulsed-field gradient (PFG) technique were performed on a Bruker AVANCE III 300 MHz spectrometer using a Diff50 gradient probe with an 8 mm ^{7}Li/^{19}F double resonance coil insert. All NMR samples were prepared in an Ar-filled glovebox and experiments were conducted at 45 °C (calibrated temperature—44.6 °C) for all samples, and at 25 °C (calibrated temperature—26.7 °C) for PEO90TO10-18Li. Polymer electrolyte samples were packed into a 4 mm NMR zirconia rotor which was then placed into a thoroughly dried 5 mm Shigemi microtube. The PFG measurements were achieved with the bipolar-gradient pulse stimulated-echo sequence (BPP-STE) with longitudinal eddy current delay (LED)[55]. A linear 16-step gradient ramp was used in each experiment with the maximum gradient strength at 272,500 and 100,000 G m^{-1} for ^{7}Li and ^{19}F measurements, respectively. The gradient pulse length (δ) was set from 1.3 to 2.5 ms depending on the T_2 relaxation time of the samples. For all measurements, the diffusion time (Δ) was set to 200 ms. Diffusion coefficients were extracted by fitting the PFG signal attenuation curves using the Bruker NMR software "TopSpin 4.1.0", with the Stejskal-Tanner equation with the required modifications for BPP-STE pulse sequences[56].

General procedure for LFP@C surface modifications. In a round bottom flask containing a magnetic stir bar, LPF@C powder (1 g) was dispersed in MeCN (30 mL) and 1,4-diaminobenzene (0.9 g) was added. To help with dissolution and dispersion, the reaction mixture was place in an ultrasound bath for 10 min, then, under stirring, *tert*-butylnitrite (1.0 mL) was added. The reaction was stirred overnight at room temperature, then centrifugated. The recovered slurry was washed 10 times with MeOH, then 3 times with acetone to ensure the removal of unreacted compounds. The powder (NH_2 surface modified LFP@C) was then dried under vacuum overnight. Meanwhile, the copolymer (1 g) was bathed in MeOH (20 mL) overnight to ensure the presence of –OH end-group on the chains, then dried under vacuum overnight. The resulting polymeric material was then added to a round bottom flask in a nitrogen-filled glovebox and NaH (30 mg) was added. Out of the glovebox, but still under inert atmosphere, dry THF (20 mL) was added to the reaction mixture, which was consequently stirred at room temperature for 1 h. Succinic anhydride (10 mg) dissolved in dry THF (5 mL) was then added to the mixture and stirred overnight. The reaction mixture was then quenched with MeOH (10 mL), then precipitated in hexanes and dried under vacuum overnight to give a polymeric material with COOH end group. This functionalized copolymer was then dissolved in dry DMSO (30 mL) in a round bottom flask, to which DCC (100 mg) was added and dissolved. This mixture was left to stir under inert atmosphere for 30 min, then the NH_2 surface modified LFP@C particles (1 g) were quickly added. The reaction mixture was left to stir at room temperature overnight, then centrifugated and washed (10× with 30 mL DMSO, 5× with 30 mL MeOH, and 3× with 30 mL acetone). The resulting slurry was then dried under vacuum overnight to give a dark gray powder. The grafting amount was characterized by TGA, under air, at a temperature ramp of 10 °C min^{-1}, from 20 to 800 °C.

General procedure for battery cycling. All batteries were assembled in an Ar-filled glovebox, in CR2032 coin cell casings. First, the cathode was weighed to extract theoretical capacity, then the SPE was weighed and placed over the cathode coating. Then a lithium chips was weighed and placed on top of the SPE. This "sandwich" was then placed in the CR2032 casing, using 2 × 0.5 mm stainless steel spacers and a wavy spring ton ensure good interfacial contact within the battery. This assembly was then sealed together using a coin cell press and the batteries were then taken out of the glovebox for cycling. The coin cell batteries were cycled on a Zahner Zennium potentiostat, at constant current corresponding to the desired C-rate, with a maximum voltage of 3.75 V and a minimum voltage of 2.80 V. Five cycles were done at each C-rate. Selected C-rates for the cycling were C/24, C/12, C/6, and C/3. EIS of the batteries were done prior to any cycle, after the 1st cycle (at C/24 rate), and after the 5th cycle of each C-rate (before changing to a new C-rate) to follow the evolution of the batteries. EIS were performed between 1 Hz and 4 MHz, for up to 16 scans (until a steady state was reached). *In this work, room or ambient temperature will always refer to 25 °C.

Galvanostatic stability of SPEs. galvanostatic measurements were recorded using a Zahner Zennium galvanostat at 0.01 mA cm^{-2} of current density, with a ±1 V cut-off.

Data availability

Main data supporting the findings of this study are contained within the paper and its associated Supplementary Information. All other relevant data are available from the corresponding author upon request and in Zenodo repository at https://doi.org/10.5281/zenodo.4924741[57].

Received: 23 March 2021; Accepted: 9 July 2021;
Published online: 03 August 2021

References

1. Rutledge, G. C. In *Handbook of Polymer Crystallization*, 197–214, https://doi.org/10.1002/9781118541838.ch6 (John Wiley & Sons, Ltd, 2013).
2. Robbins, A. B. & Minnich, A. J. Crystalline polymers with exceptionally low thermal conductivity studied using molecular dynamics. *Appl. Phys. Lett.* **107**, 201908 (2015).
3. Mileva, D., Tranchida, D. & Gahleitner, M. Designing polymer crystallinity: an industrial perspective. *Polym. Cryst.* **1**, e10009 (2018).
4. Tashiro, K. In *Handbook of Polymer Crystallization* 165–196, https://doi.org/10.1002/9781118541838.ch5 (John Wiley & Sons, Ltd, 2013).
5. Haudin, J.-M. In *Handbook of Polymer Crystallization* 433–462, https://doi.org/10.1002/9781118541838.ch15 (John Wiley & Sons, Ltd, 2013).
6. Yin, J., Raegen, A., Idziak, S. H. J. & Forrest, J. A. Crystallization and melting of highly monodisperse poly(ethylene-oxide). *Soft. Matter.* **16**, 7958–7969 (2020).
7. Kripotou, S. et al. Structure and crystallization behavior of poly(ethylene oxide) (PEO) chains in core–shell brush copolymers with poly(propylene oxide)-block-poly(ethylene oxide) side chains. *Macromolecules* **49**, 5963–5977 (2016).
8. Araneda, E. et al. Crystallization behavior of PEO in blends of poly(ethylene oxide)/poly(2-vinyl pyridine)-b-(ethylene oxide) block copolymer. *Polym. Eng. Sci.* **52**, 1128–1136 (2012).
9. Sasaki, T., Miyazaki, A., Sugiura, S. & Okada, K. Crystallization of poly (ethylene oxide) from solutions of different solvents. *Polym. J.* **34**, 794–800 (2002).
10. Money, B. K. & Swenson, J. Dynamics of poly(ethylene oxide) around its melting temperature. *Macromolecules* **46**, 6949–6954 (2013).
11. Fenton, D. E., Parker, J. M. & Wright, P. V. Complexes of alkali metal ions with poly(ethylene oxide). *Polymer* **14**, 589 (1973).
12. Berthier, C. et al. Microscopic investigation of ionic conductivity in alkali metal salts-poly(ethylene oxide) adducts. *Solid State Ion.* **11**, 91–95 (1983).
13. Armand, M. Polymer solid electrolytes—an overview. *Solid State Ion.* **9–10**, 745–754 (1983).
14. Seki, S. et al. Distinct difference in ionic transport behavior in polymer electrolytes depending on the matrix polymers and incorporated salts. *J. Phys. Chem. B* **109**, 3886–3892 (2005).
15. Wang, S.-H., Hou, S.-S., Kuo, P.-L. & Teng, H. Poly(ethylene oxide)-co-poly (propylene oxide)-based gel electrolyte with high ionic conductivity and mechanical integrity for lithium-ion batteries. *ACS Appl. Mater. Interfaces* **5**, 8477–8485 (2013).
16. Li, M. et al. Polymeric ionic liquid membranes as electrolytes for lithium battery applications. *J. Appl. Electrochem.* **42**, 851–856 (2012).
17. Jin, X. et al. Stretchable supercapacitor at −30 °C. *Energy Environ. Sci.* **14**, 3075–3085 (2021).
18. Li, Y. et al. Hexagonal boron nitride induces anion trapping in a polyethylene oxide based solid polymer electrolyte for lithium dendrite inhibition. *J. Mater. Chem. A* **8**, 9579–9589 (2020).
19. Wang, H. et al. Mechanical property-reinforced PEO/PVDF/$LiClO_4$/SN blend all solid polymer electrolyte for lithium ion batteries. *J. Electroanal. Chem.* **869**, 114156 (2020).
20. Li, Y. et al. Poly(ionic liquid)-polyethylene oxide semi-interpenetrating polymer network solid electrolyte for safe lithium metal batteries. *Chem. Eng. J.* **375**, 121925 (2019).
21. Rosa, C. D. & Auriemma, F. In *Handbook of Polymer Crystallization* 31–72, https://doi.org/10.1002/9781118541838.ch2 (John Wiley & Sons, Ltd, 2013).
22. Flory, P. J. Theory of crystallization in copolymers. *Trans. Faraday Soc.* **51**, 848–857 (1955).
23. Flory, P. J. On the morphology of the crystalline state in polymers. *J. Am. Chem. Soc.* **84**, 2857–2867 (1962).
24. Weeks, J. J. Melting temperature and change of lamellar thickness with time for bulk polyethylene. *J. Res. Natl. Bur. Stand. Sect. Phys. Chem.* **67A**, 441 (1963).
25. Hoffman, J. D. & Lauritzen, J. I. Crystallization of bulk polymers with chain folding: theory of growth of lamellar spherulites. *J. Res. Natl. Bur. Stand. Sect. Phys. Chem.* **65A**, 297 (1961).
26. Skupov, K. M., Piche, L. & Claverie, J. P. Linear polyethylene with tunable surface properties by catalytic copolymerization of ethylene with *N* -vinyl-2-pyrrolidinone and *N* -Isopropylacrylamide. *Macromolecules* **41**, 2309–2310 (2008).
27. Lehman, S. E. et al. Linear copolymers of ethylene and polar vinyl monomers via olefin metathesis−hydrogenation: synthesis, characterization, and comparison to branched analogues. *Macromolecules* **40**, 2643–2656 (2007).
28. Butzelaar, A. J. et al. A systematic study of vinyl ether-based poly(ethylene oxide) side-chain polymer electrolytes. *ACS Appl. Polym. Mater.* https://doi.org/10.1021/acsapm.0c01398 (2021).
29. Shapiro, Y. E. Analysis of chain microstructure by ^{1}H and ^{13}C NMR Spectroscopy. *Bull. Magn. Reson.* **7**, 27–58 (1985).
30. Bovey, F. A. Configurational sequence studies by n.m.r. and the mechanism of vinyl polymerization. *Pure Appl. Chem.* **15**, 349–368 (1967).
31. Blankenburg, J. et al. The poly(propylene oxide-co-ethylene oxide) gradient is controlled by the polymerization method: determination of reactivity ratios by direct comparison of different copolymerization models. *Polym. Chem.* **10**, 2863–2871 (2019).
32. Gronski, W., Hellmann, G. & Wilsch-Irrgang, A. ^{13}C NMR characterization of ethylene oxide/propylene oxide adducts. *Makromol. Chem.* **192**, 591–601 (1991).
33. Roux, C. & Sanchez, J.-Y. Ionic conductivities of PPO-LiTFSI complexes. *Solid State Ion.* **72**, 160–164 (1994).
34. Devaux, D., Bouchet, R., Glé, D. & Denoyel, R. Mechanism of ion transport in PEO/LiTFSI complexes: effect of temperature, molecular weight and end groups. *Solid State Ion.* **227**, 119–127 (2012).
35. Zhang, H. et al. Lithium bis(fluorosulfonyl)imide/poly(ethylene oxide) polymer electrolyte. *Electrochimica Acta* **133**, 529–538 (2014).
36. Stolwijk, N. A. et al. Salt-concentration dependence of the glass transition temperature in PEO–NaI and PEO–LiTFSI polymer electrolytes. *Macromolecules* **46**, 8580–8588 (2013).
37. Daigle, J.-C. et al. Lithium battery with solid polymer electrolyte based on comb-like copolymers. *J. Power Sources* **279**, 372–383 (2015).
38. Olmedo-Martínez, J., Meabe, L., Basterretxea, A., Mecerreyes, D. & Müller, A. Effect of chemical structure and salt concentration on the crystallization and ionic conductivity of aliphatic polyethers. *Polymers* **11**, 452 (2019).
39. Foran, G. et al. The impact of absorbed solvent on the performance of solid polymer electrolytes for use in solid-state lithium batteries. *iScience* **23**, 101597 (2020).
40. Ren, X. et al. Flexible nanofiber-reinforced solid polymer lithium-ion battery. *Energy Technol.* **7**, 1900064 (2019).
41. Carvalho, L. M., Guégan, P., Cheradame, H. & Gomes, A. S. Variation of the mesh size of PEO-based networks filled with TFSILi: from an Arrhenius to WLF type conductivity behavior. *Eur. Polym. J.* **36**, 401–409 (2000).
42. Messinger, R. J., Huynh, T. V., Bouchet, R., Sarou-Kanian, V. & Deschamps, M. Magic-angle-spinning-induced local ordering in polymer electrolytes and its effects on solid-state diffusion and relaxation NMR measurements. *Magn. Reson. Chem.* **58**, 1118–1129 (2020).
43. Lu, Y. et al. Stable cycling of lithium metal batteries using high transference number electrolytes. *Adv. Energy Mater.* **5**, 1402073 (2015).
44. Cao, D. et al. Lithium dendrite in all-solid-state batteries: growth mechanisms, suppression strategies, and characterizations. *Matter* **3**, 57–94 (2020).
45. Molinari, N., Mailoa, J. P. & Kozinsky, B. Effect of salt concentration on ion clustering and transport in polymer solid electrolytes: a molecular dynamics study of PEO–LiTFSI. *Chem. Mater.* **30**, 6298–6306 (2018).
46. Shamsipur, M. & Popov, A. I. Lithium-7 NMR study of the kinetics of Li+ ion complexation by C222 and C221 cryptates in acetonitrile, propylene carbonate, and acetone solutions. *J. Phys. Chem.* **90**, 5997–5999 (1986).
47. Chintapalli, M. et al. Relationship between conductivity, ion diffusion, and transference number in perfluoropolyether electrolytes. *Macromolecules* **49**, 3508–3515 (2016).
48. Hsieh, C.-T., Pai, C.-T., Chen, Y.-F., Chen, I.-L. & Chen, W.-Y. Preparation of lithium iron phosphate cathode materials with different carbon contents using glucose additive for Li-ion batteries. *J. Taiwan Inst. Chem. Eng.* **45**, 1501–1508 (2014).
49. Choi, D. & Kumta, P. N. Surfactant based sol–gel approach to nanostructured $LiFePO_4$ for high rate Li-ion batteries. *J. Power Sources* **163**, 1064–1069 (2007).
50. Placke, T., Kloepsch, R., Dühnen, S. & Winter, M. Lithium ion, lithium metal, and alternative rechargeable battery technologies: the odyssey for high energy density. *J. Solid State Electrochem.* **21**, 1939–1964 (2017).
51. Delaporte, N., Perea, A., Amin, R., Zaghib, K. & Bélanger, D. Chemically grafted carbon-coated $LiFePO_4$ using diazonium chemistry. *J. Power Sources* **280**, 246–255 (2015).
52. Sahore, R. et al. Practical considerations for testing polymer electrolytes for high-energy solid-state batteries. *ACS Energy Lett.* **6**, 2240–2247 (2021).
53. Hamaide, T., Spitz, R., Letourneux, J. P., Clavene, J. & Guyot, A. Heterogeneous catalysis for ring opening anionic oligomerisation. *Macromol. Symp.* **88**, 191–200 (1994).
54. Pożyczka, K., Marzantowicz, M., Dygas, J. R. & Krok, F. Ionic conductivity and lithium transference number of poly(ethylene oxide):LiTFSI system. *Electrochimica Acta* **227**, 127–135 (2017).
55. Wu, D. H., Chen, A. D. & Johnson, C. S. An improved diffusion-ordered spectroscopy experiment incorporating bipolar-gradient pulses. *J. Magn. Reson. A* **115**, 260–264 (1995).
56. Stejskal, E. O. & Tanner, J. E. Spin diffusion measurements: spin echoes in the presence of a time-dependent field gradient. *J. Chem. Phys.* **42**, 288–292 (1965).

57. St-Onge, V., Cui, M., Rochon, S., Daigle, J.-C. & Claverie, J. Reducing crystallinity in solid polymer electrolytes for lithium-metal batteries via statistical copolymerization. https://doi.org/10.5281/zenodo.4924741 (2021).

Acknowledgements

V.S.O. and J.P.C. acknowledge support by the MITACS organization and the Canada Research Chair program. This work was supported by the MITACS organization and by Hydro-Québec, the Canada Foundation for Innovation and by the Natural Sciences and Engineering Research Council of Canada. We also thank Pre Gillian Goward, from McMaster University, for her help regarding the PFG SSNMR measurements.

Author contributions

Vincent St-Onge performed all experiments excepted the solid-state NMR experiments (performed by Mengyang Cui) and the DSC measurements (performed by Sylviane Rochon). Jerome P. Claverie designed the initial idea of research. Vincent St-Onge, Jerome P. Claverie, and Jean-Christophe Daigle were responsible for project evolution. Vincent St-Onge and Jerome P. Claverie wrote the paper, with input and revisions from all authors.

Competing interests

The authors declare no competing interests.

Additional information

Supplementary information The online version contains supplementary material available at https://doi.org/10.1038/s43246-021-00187-2.

Correspondence and requests for materials should be addressed to J.P.C.

Peer review information *Communications Materials* thanks Yanfeng Zhang and the other, anonymous, reviewer for their contribution to the peer review of this work. Primary Handling Editor: John Plummer. Peer reviewer reports are available.